Surface morphology and structure of epitaxial yttrium on niobium buffer layers with different orientations

2000 J. Phys.: Condens. Matter 12 4675

(http://iopscience.iop.org/0953-8984/12/22/301)

J. Phys.: Condens. Matter **12** (2000) 4675–4686. Printed in the UK PII: S0953-8984(00)10137-7

Surface morphology and structure of epitaxial yttrium on niobium buffer layers with different orientations

B Krause† and K Theis-Bröhl

Institut für Experimentalphysik/Festkörperphysik, Ruhr-Universität Bochum, D-44780 Bochum, Germany

Received 7 December 1999

Abstract. We report temperature- and substrate-dependent growth studies of epitaxial yttrium films. Using three different sapphire orientations and Nb buffers, Y was grown in the (0001), $(10\bar{1}1)$ and $(10\bar{1}2)$ crystal orientations. Atomic force microscopy and x-ray measurements were used to study the topography and structural properties of the samples. Whereas the Y(0001) films show a high crystallinity and a small surface roughness, Y$(10\bar{1}1)$ and Y$(10\bar{1}2)$ films have regularly structured surfaces with a lower crystalline quality. Temperature and thickness studies show a strong dependence of the surface morphology on growth temperature and film thickness.

1. Introduction

During the past few decades, molecular beam epitaxy (MBE) has become an important method for preparing high-quality epitaxial thin films and multilayers. This has led to exciting new results in research fields such as electronic properties, phase transitions and magnetism in reduced dimensions. The nonequilibrium growth process involving competing interactions which determine the crystal structure and surface morphology of the films remains in itself an important research topic. Even with perfect control of the structural properties, it is often difficult or impossible to predict the physical properties of a sample.

Temperature- and substrate-dependent growth studies of yttrium promise new information about the epitaxial growth of hcp metals. Epitaxial hcp crystals are less well studied than cubic systems because of their complex geometry. Few systematic studies of MBE-grown hcp crystals on bcc substrates have been reported [1–4]. The growth of hcp yttrium is important for several reasons: yttrium is a nonmagnetic material that exhibits a similar structure to many rare-earth (RE) metals [5]. Therefore, for initiating the single-crystal growth yttrium films often serve as seed layers for RE thin films and superlattices [6]. Furthermore, they are often used for studies of multilayer exchange coupling in RE superlattices [1, 3, 6, 7]. Structure and magnetic behaviour cannot be treated separately in superlattices. For example, lattice clamping in Dy/Y multilayers suppresses the transition from the helimagnetic to the ferromagnetic phase which is typical for bulk Dy [7]. Furthermore, yttrium itself has some astounding characteristics: upon loading with hydrogen it switches reversibly from the metallic YH_2 phase to the insulator YH_3 phase [8–10]. The phases differ drastically in their electronic and optical properties, opening up new technological possibilities such as optical switches and hydrogen sensors.

To understand these complex systems it is indispensable to master the epitaxial growth of different Y thin-film orientations by means of molecular beam epitaxy. Up to now, most

† Present address: Max-Planck-Institut für Metallforschung, Heisenbergstrasse 1, D-70569 Stuttgart, Germany.

0953-8984/00/224675+12$30.00

growth studies have been devoted to Y(0001) on bcc(110), often using Nb and Ta buffer layers grown on $(11\bar{2}0)$ sapphire surfaces [1,3,7]. Recent experiments give insight into the growth of faceted $Y(10\bar{1}2)$ on $Nb(211)/Al_2O_3(10\bar{1}0)$ [3, 7, 11]. In addition, preliminary measurements confirm the existence of single-crystalline $Y(10\bar{1}1)$ on $Nb(100)/Al_2O_3(10\bar{1}2)$. For the present study we prepared a set of $Nb/Y/Nb/Al_2O_3$ samples in order to compare the three different film orientations under the same growth conditions while only the substrate orientation is changed. This direct comparison between different hcp growth orientations gives insight into general growth mechanisms and the compensation of strain in thin films.

2. Growth of yttrium on niobium

Generally, epitaxy is supported by similar structures of substrate and film. Although Y and Nb possess different structures and lattice parameters, epitaxial growth of hcp Y ($a_Y = 3.6474$ Å, $c_Y = 5.7306$ Å) on bcc Nb ($a_{Nb} = 3.307$ Å) can be achieved in several crystal orientations. Strain compensates for a small lattice misfit between substrate and epilayer up to a critical thickness, while large misfit leads to dislocations at the interface or to polycrystalline growth. Therefore epitaxy depends in a complicated way on various energies (interfacial, surface, strain and dislocation).

Two epitaxial systems have been studied in detail in the past:

(i) **hcp(0001) on bcc(110)**. Y(0001)/Nb(110) exhibits the Nishiyama–Wasserman orientation (figure 1). In this configuration $Y[11\bar{2}0] \parallel Nb[001]$ while $Y[\bar{1}100] \parallel Nb[1\bar{1}0]$. The perpendicular directions $[11\bar{2}0]$ and $[\bar{1}100]$ have misfits of 10.3% and 35.1% respectively, with respect to the Nb substrate. Growth of single-crystal films is only possible because of the 3:4 supercommensurability with a misfit of 1.3% between three Y and four Nb surface meshes along $[\bar{1}100]$ [1]. In this system the high structural order of the hcp layer is supported by the preferred close-packed [0001] direction. In contrast, Y[0001]/Nb[111] with the same 3:4 supercommensurability is less ordered because of the larger misfit of 3.7%.

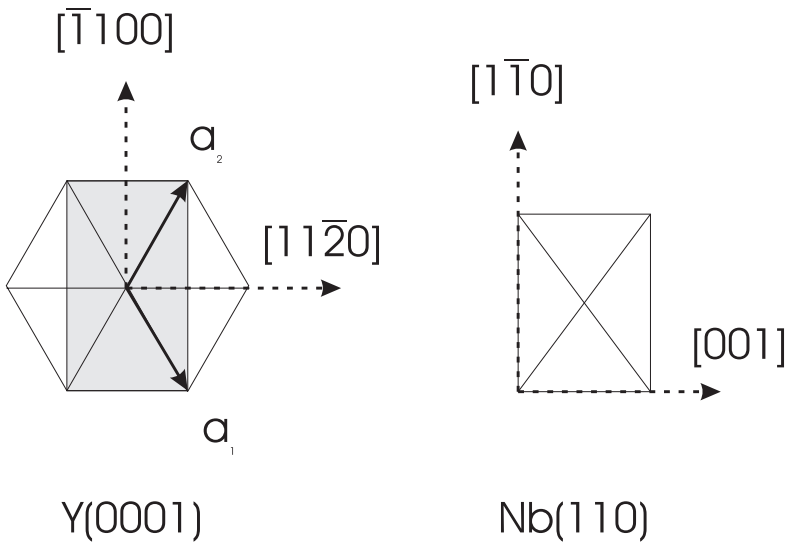

Figure 1. The epitaxial relationship of Y(0001) on Nb(110).

(ii) **hcp(10$\bar{1}$2) on bcc(211)**. Y(10$\bar{1}$2) grows tilted on Nb(211) with a tilt angle $\alpha = 4.3^\circ$ along Nb[$\bar{1}$11] [3, 7]. Tilted growth is typical for hcp(10$\bar{1}$2) on bcc(211) and was observed in detail in different hcp and bcc systems [2, 3, 7, 11]. A model was developed explaining the tilt by dislocation gliding along the glide plane Y(0001). Without tilt the misfit would be $f = -8.8\%$. It is possible to calculate the tilt angle by simple geometric considerations which assume commensurable growth without stress. Two equivalent tilt directions exist, namely Nb[$\bar{1}$11] and Nb[1$\bar{1}\bar{1}$]. One of them can be suppressed by using a miscut substrate. The tilt-induced (10$\bar{1}$2) surface has a high surface energy. To reduce its energy, facets are usually produced at the surface. Frequently the facets are limited by Y(10$\bar{1}$2) and Y(10$\bar{1}$3) including the facet angle $\alpha = 11.048^\circ$ [3, 7].

Our work has revealed a new epitaxial Y/Nb system: Y(1$\bar{1}$01)/Nb(100). The (10$\bar{1}l$) planes, $l = 0, 1, 2, \ldots, n$, are closely related. A change from Y(1$\bar{1}$0n) to Y(1$\bar{1}$0($n+1$)) only requires inserting an element of the Y(0001) plane with the width $d_Y = (\sqrt{3}/2)a_Y$. Because of the remarkable similarity of the (10$\bar{1}l$) crystal planes, it is sensible to expect structural similarities between the Y(10$\bar{1}$1) and Y(10$\bar{1}$2) surfaces, and the geometrical models developed for (10$\bar{1}$2) may be transferred to (10$\bar{1}$1). Assuming an in-plane orientation of Y and Nb as indicated in figure 2, the misfit $f_\perp$ along [11$\bar{2}$0] of 10.2% and the orthogonal misfit of -1% lead to an energetically unfavourable situation. The stress due to $f_\perp$ can be released by the gliding mechanism presumed for Y(10$\bar{1}$2), resulting in a regular net of dislocations. Figure 3 shows

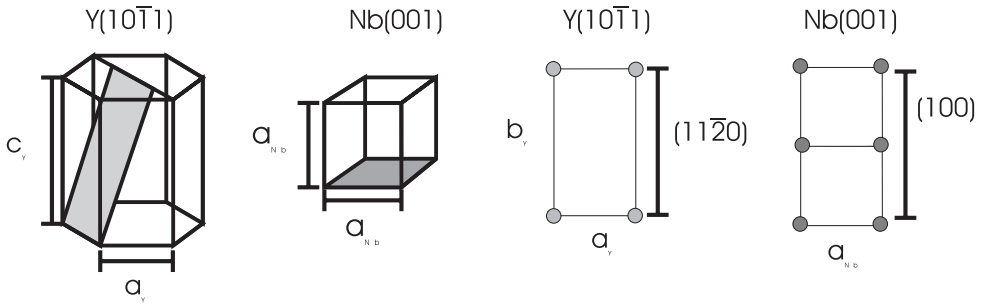

Figure 2. The orientation of the parallel-growing Y(10$\bar{1}$1) and Nb(100) planes in their unit cell. The right-hand side represents the surface meshes and the parallel Nb(010) and Y(11$\bar{2}$0) planes perpendicular to the growth direction.

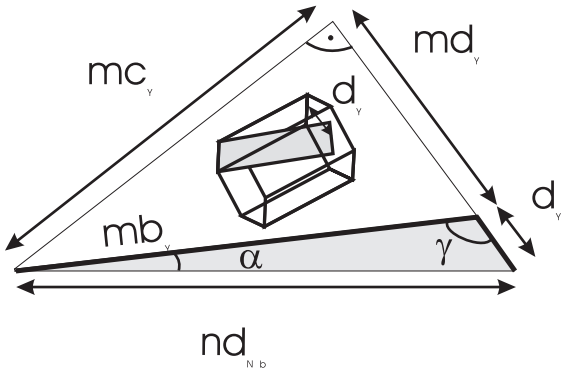

Figure 3. The geometric model explaining the tilt on Y(10$\bar{1}$1). The diagram shows the section between two dislocations.

a geometrical construction in analogy with the model used by Du *et al* [11] to predict the tilt angle of Y(10$\bar{1}$2). Commensurability between n Nb and m Y meshes can be produced by inserting an element of the Y(0001) plane with the width d_Y after m Y meshes. This model leads to the following geometrical relationships:

$$(nd_{Nb})^2 = ((m+1)d_Y)^2 + (mc_Y)^2 \tag{1}$$

$$\frac{d_Y}{\sin\alpha} = \frac{nd_{Nb}}{\sin\gamma} \tag{2}$$

and

$$\frac{mc_Y}{\sin(180^\circ - \gamma)} = \frac{mb_Y}{\sin 90^\circ} \tag{3}$$

with the length of the Y surface mesh given by $b_Y = \sqrt{(3/4)a_Y^2 + c_Y^2}$, and the length of the Nb surface mesh $d_{Nb} = a_{Nb}$ in the tilt direction. As a consequence of the small misfit between one Y and two Nb meshes ($b_Y = 6.5435$ Å, $2a_{Nb} = 6.614$ Å) we set $m = 2n$ following Du *et al* [11]. With $\lambda = c_Y/a_Y$ one gets the expression

$$\frac{1}{\sin\alpha} = \frac{a_{Nb}}{c_Y} n \sqrt{1 + \lambda^2 \frac{4}{3}} \tag{4}$$

for calculating the tilt angle α. The Nb mesh number n results from

$$n = \frac{1}{Z}(1 + \sqrt{1 + 2Z}) \tag{5}$$

with

$$Z = \frac{8a_{Nb}^2}{3a_Y^2}\left[1 - \frac{3a_Y^2}{16a_{Nb}^2}\left(1 + \lambda^2\frac{4}{3}\right)\right]. \tag{6}$$

From this model we calculate $\alpha = 1.197^\circ$ and $n = 2m = 40$ for the growth of Y(10$\bar{1}$1) on Nb(001).

3. Sample preparation

For our study we employed α-Al_2O_3 with different orientations as substrates. X-ray measurements reveal a miscut of 2.09° for Al_2O_3(11$\bar{2}$0), 0.06° for Al_2O_3(10$\bar{1}$0) and 0.60° for Al_2O_3(10$\bar{1}$2). We prepared a set of Nb/Y/Nb/Al_2O_3 samples in the temperature range 400–600 °C, consisting of a 300 Å Nb buffer, a 300 Å Y film and a 100 Å Nb cap layer, the latter present for oxidation protection. To maintain identical growth conditions for the different sample orientations, including identical growth temperature, layer thickness and residual gas pressure, we used a sample holder accepting up to five different substrates. All sapphires were annealed at 400–600 °C for 1–2 h in a residual gas pressure of 10^{-7}–10^{-8} mbar. Subsequently, they were annealed at 300 °C for 14 h under UHV conditions followed by a short heat treatment at 1100 °C prior to growth. Nb and Y were deposited by electron beam evaporation. The optimal deposition rate for all layers proved to be 0.5 Å s^{-1}. The 300 Å thick Nb buffer was deposited with a substrate temperature of 900 °C, and subsequently annealed at 950 °C for 20 min. After cooling down to a temperature in the range of 400–600 °C, 300 Å thick Y layer was deposited. This layer was covered by a 100 Å Nb cap layer at 200 °C. We monitored the sample preparation *in situ* by reflection high-energy electron diffraction (RHEED) to ensure the crystalline quality of the samples.

For the subsequent interpretation of our data some explanations concerning the influence of the Nb cap layer are in order. It is well known that Nb develops an oxide layer in air, with a

thickness of 20 Å, whereas the oxidation of Y has not been studied up to now. Consequently the Nb cap layer enables a controlled sample architecture to be maintained. To diminish the main disadvantage of a cap layer, i.e. burying the Y surface morphology, the cap layer deposition took place at 200 °C. The low growth temperature for Nb, far away from the optimal growth temperature of 900 °C, results in a small surface diffusion. We estimate the surface self-diffusion coefficient according to Flynn [14] at $T = 200$ °C (475 K):

$$D_S(T) \approx 10^{-3} 10^{-3T_S/(2T)} \text{ cm}^2 \text{ s}^{-1} \approx 10^{-12} \text{ cm}^2 \text{ s}^{-1} \tag{7}$$

where T_S is the melting temperature. Thus the surface diffusion coefficient differs widely from the presumed lower limit $D_S \approx 10^{-7}$ cm^2 s^{-1} for optimal growth [14]. Therefore the Nb cap layer buries surface structures of the Y layer on an atomic scale, while the nanoscale morphology is imprinted on the Nb layer. The Nb surface roughness separates into an intrinsic part and an additional part caused by the Y layer.

Ex situ we performed atomic force microscopy (AFM) measurements examining the surface morphology and x-ray measurements studying the epitaxy and crystallinity of the samples.

4. Structural measurements

Figure 4 presents representative AFM topographs obtained in contact mode of samples with identical architectures but different substrate orientations and growth temperatures. Every image covers an area of 2.5 × 2.5 μm in order to facilitate comparison of the length scale of the observed surface morphologies. We obtain quantitative information from the root mean square (rms) roughness as presented in figure 5, while the statements concerning the geometric surface morphology are supported by line scans. To improve the meaningfulness of the rms roughness measured by AFM we provide the mean values of 4–5 different topographs of area 5 × 5 μm^2 taken at different sample positions.

The samples deposited on Nb(110)/Al_2O_3(11$\bar{2}$0) possess a small surface roughness of 3–4 monolayers (ML), which is typical for MBE-grown Nb layers for the given deposition conditions. For the temperature range investigated the surface roughness is independent of the Y growth temperature (figure 5). The AFM pictures contain small, approximately self-similar surface morphologies. This implies that the Nb-covered Y layer may only exhibit even smaller surface morphologies, which are washed out by the intrinsic roughness of the cap layer dominating the AFM topographs. In contrast, the other growth orientations, Y(10$\bar{1}$1)/Nb(100) and Y(10$\bar{1}$2)/Nb(211), show regularly structured surfaces. They change in size with growth temperature while the general shape remains the same. For both orientations the structures are aligned along a preferred direction with respect to the crystal planes of the sapphire substrate. The structure size increases roughly exponentially with Y deposition temperature as indicated by their lateral dimension and rms roughness. For substrate temperatures up to 450 °C the roughness of the structured surfaces is of the same order as that of the unstructured surfaces but slightly larger. Surprisingly, for Y(10$\bar{1}$2)/Nb(211) deposited at 600 °C the roughness is equivalent to half of the nominal Y-layer thickness. Together with the known faceted surface of Y on Nb(211) [7, 11] this confirms the assumption that the surface morphologies result from a faceted Y layer and not from the 100 Å Nb cap layer. From RHEED measurements we found no indication that the Nb(211) and Nb(100) buffer layers exhibit facets which could lead to misinterpretation. Line scans as indicated in figure 6 reveal the geometry of the facets. On Nb(211)/Al_2O_3(10$\bar{1}$0) the Y regular facets are formed like a roof, limited by two surfaces including an angle of 10–13°. Compared to the theoretical value of 11.048° this gives an upper value for the change induced by the cap layer. The measured angles show only a small

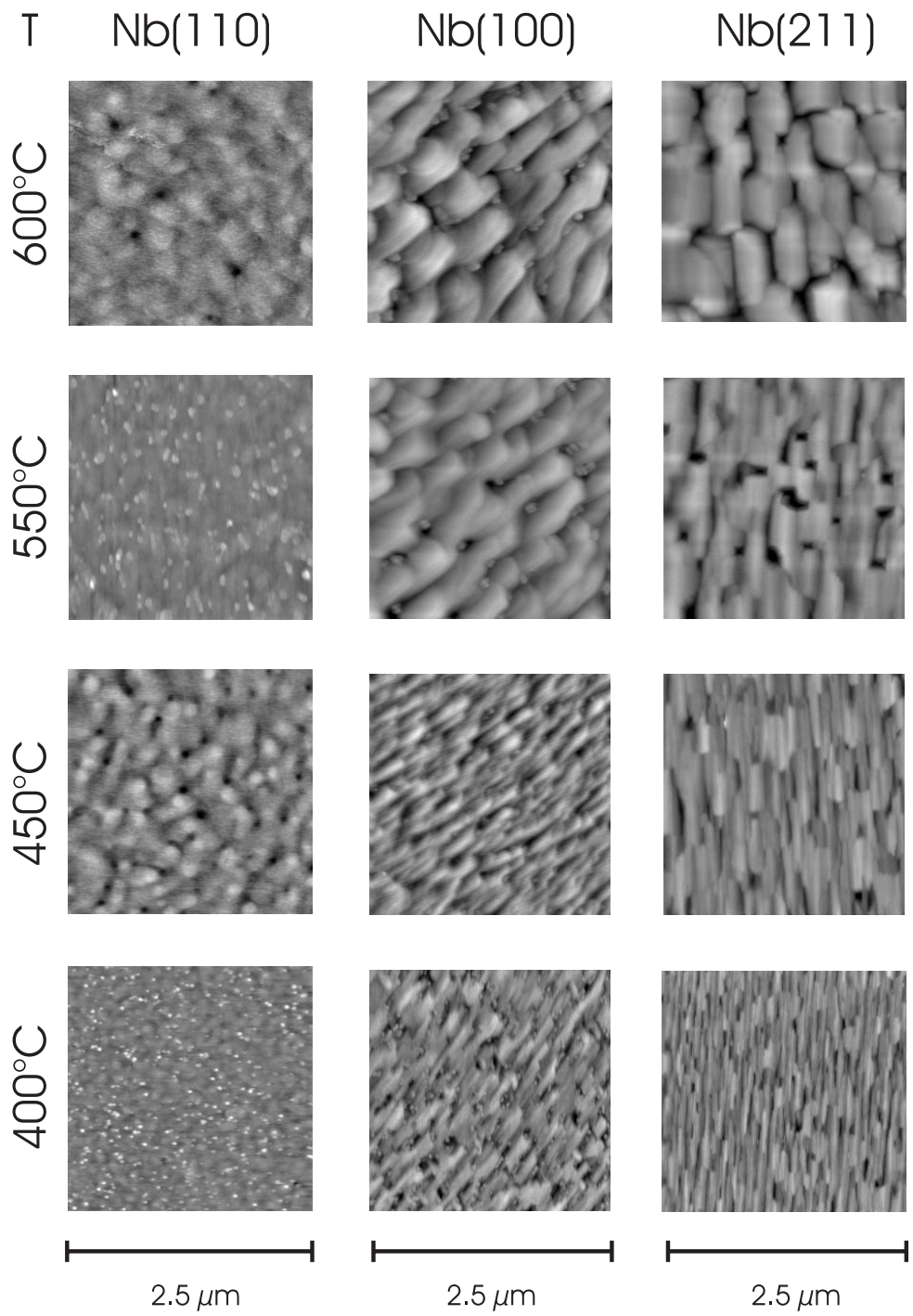

Figure 4. A survey of the AFM measurements. The columns show samples which are grown on the same substrate but with different Y growth temperatures while the rows present samples which are grown on different substrate orientations but under different growth conditions.

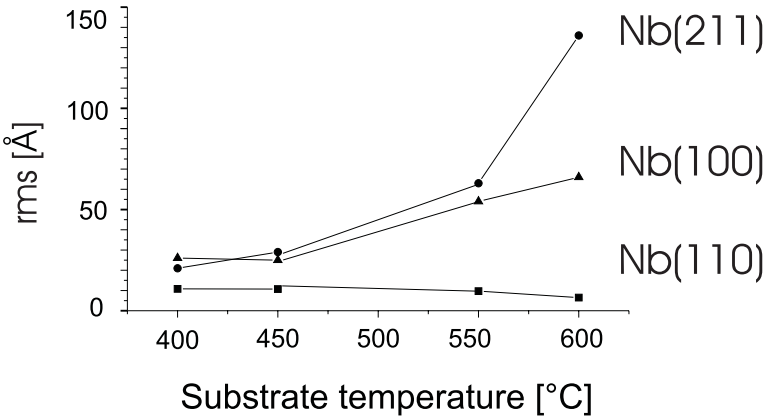

Figure 5. The surface roughness of the samples, depending on substrate temperature and substrate orientation.

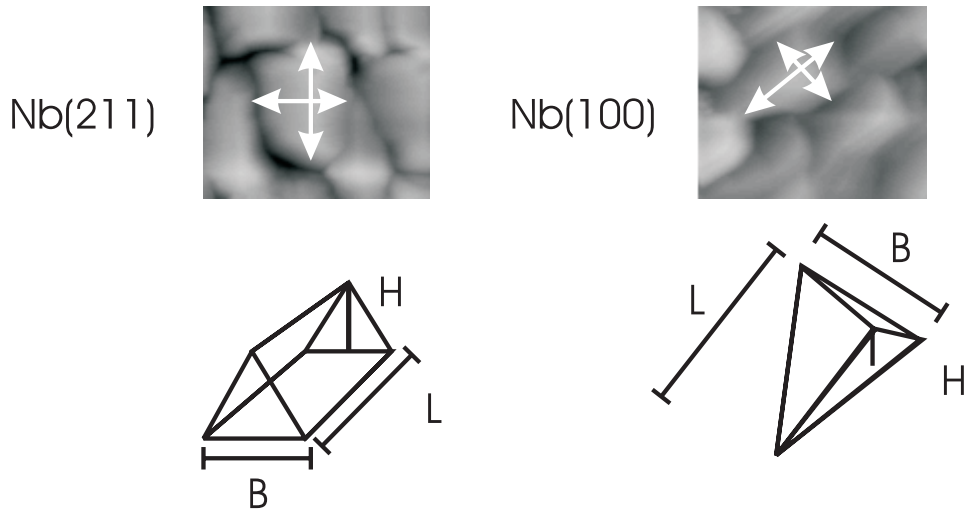

Figure 6. Typical line measurements along preferred directions of the facets and the resulting facet structure. On Nb(211) the facets seem to be rooflike, while Nb(100) induces pyramid-like structures.

deviation from the theoretical value. That leads to the conclusion that the cap layer changes the sample morphology only slightly. However, for Nb(100)/$Al_2O_3(10\bar{1}2)$ one obtains pyramid-like facets with the typical angles $\alpha = 14 \pm 5^\circ$, $\beta = 9 \pm 3^\circ$ parallel to $\boldsymbol{L}$ and parallel to $\boldsymbol{B}$, respectively.

4.1. X-ray measurements

We have analysed the structural properties of our films by means of x-ray diffraction and reflectivity. For these studies Cu Kα radiation ($\lambda = 0.542$ Å) from a rotating anode source with a graphite (111) monochromator was used. The specular reflectivity and the diffuse scattering give additional information concerning the sample surface, and the interface structure, as well

as the nature of the facets. As an example, figure 7 reproduces measurements of the specular reflectivity of Nb/Y/Nb/Al_2O_3, Y being deposited at 400 °C. Fits to the measurements based on the multilayer sample structure are also shown. The fit program is based on the Parratt formalism [20], including optical corrections due to resolution and sample geometry. They are offset from the experimental data for reasons of clarity. While the Y(0001)/Nb($\bar{1}$10) sample exhibits many small film thickness oscillations, the oscillations relating to Y/10$\bar{1}$1)/Nb(100) and Y(10$\bar{1}$2)/Nb(211) are strongly damped and dominated by the Nb buffer layer. From the fits we know that in all cases the Nb buffer layer has a roughness of 4–10 Å. Y(0001)/Nb(110) shows the same roughness as the buffer layer. In contrast to this the roughness of Y(10$\bar{1}$1) and Y(10$\bar{1}$2) is extremely high and can only be fitted for lower growth temperatures. For the samples presented in figure 7 we obtain roughness values of $\sigma_{Y(10\bar{1}1)} \approx 15$ Å and $\sigma_{Y(10\bar{1}2)} \approx 20$ Å. The Nb cap layer cannot be separated exactly, but the roughness is of the same order as the roughness of the underlying Y layer.

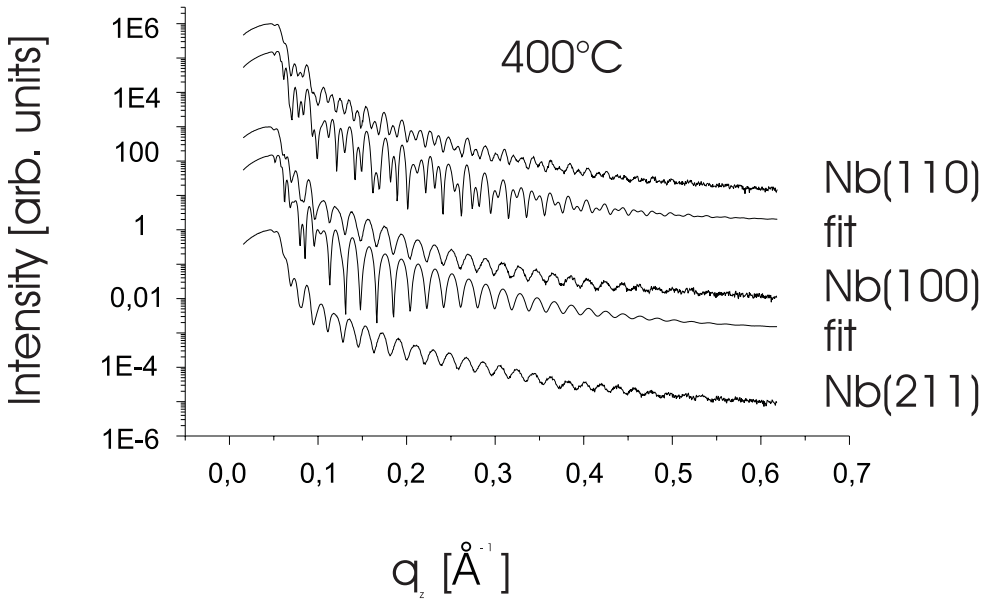

Figure 7. Comparison of the x-ray reflectivities of the samples with 400 °C Y deposition temperature. Additionally, two fits are represented relating to the samples with Nb(110) and Nb(100) buffers.

In figure 8 measurements of the specular and diffuse scattering from the samples deposited on Nb(211) at 500 °C are reproduced. The first measurement (a) was performed with the scattering plane perpendicular to the facet ridges, the second (b) with the scattering plane in the orthogonal direction. Both measurements reveal oscillations of the specular reflectivity framed between the 'Yoneda' wings. In addition to this the second measurement (b) reveals correlated intensity as revealed by a corresponding distance of $d = 300 \pm 40$ nm. Perpendicular to the facets the diffuse intensity is stronger but not correlated. Measurements of the diffuse background of a Y(10$\bar{1}$1)/Nb(100) sample deposited at 550° show no correlated intensity in the same direction.

According to the high-angle x-ray analysis of Y(10$\bar{1}$1)/Nb(100), the Y structure depends strongly on the Y deposition temperature. All samples exhibit a Y(10$\bar{1}$1) peak tilted with respect to the Nb crystal planes, which themselves are tilted by 2.8° relative to the sapphire

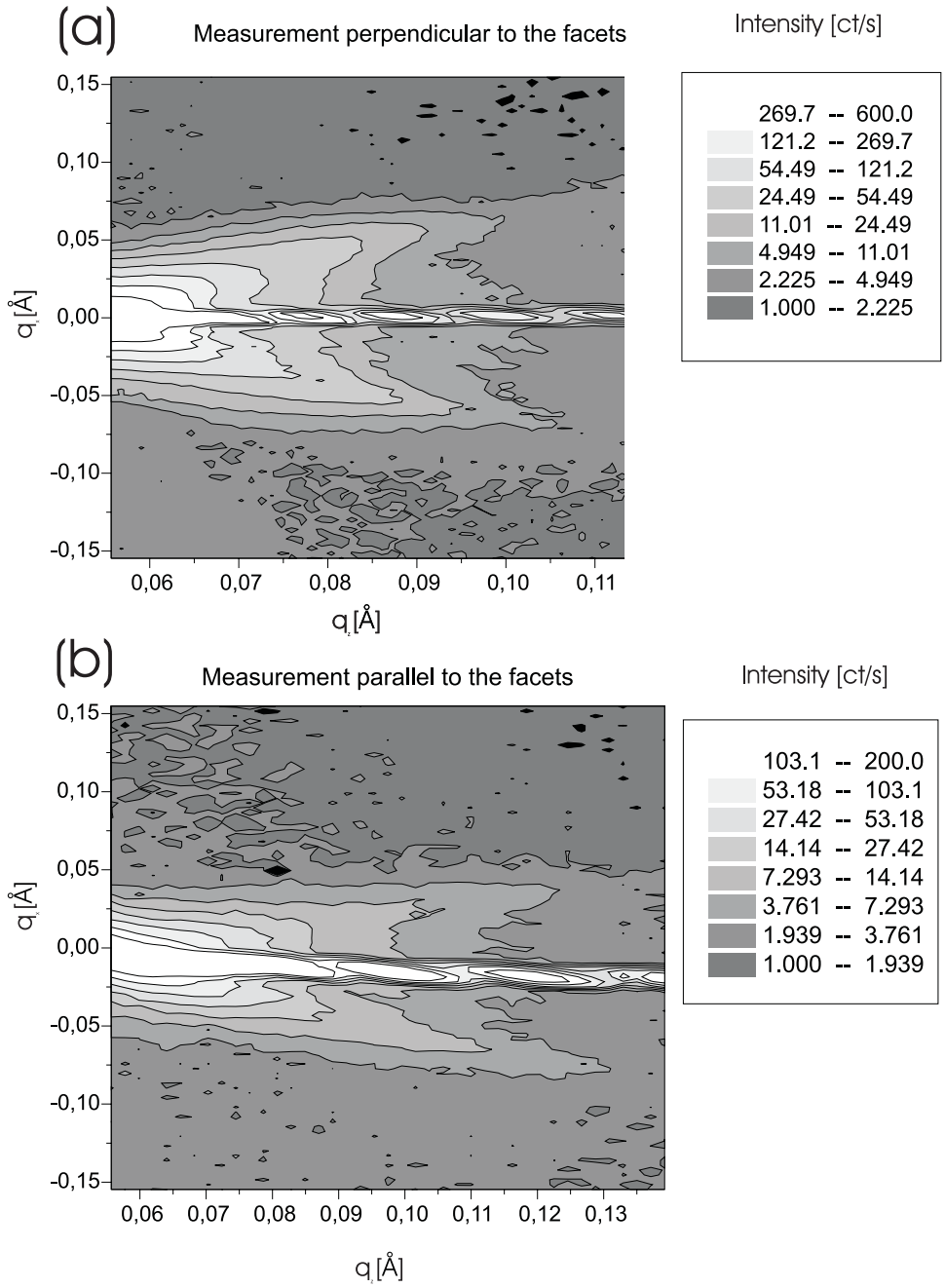

Figure 8. Logarithmic specular and diffuse scattering intensity for small angles, measured at the sample prepared at 550 °C on Nb(211).

substrate [15]. The maximum tilt directions for the two layers are the same. For Y($10\bar{1}1$) deposited at 450 °C, the maximal tilt relative to the Nb lattice planes is 2°. Radial scans through the Y($10\bar{1}1$) peak contain an additional Y(0001) peak for substrate temperatures up

to 500 °C. We suggest that for low temperatures in some domains the $(10\bar{1}1)$ direction is replaced by the close-packed (0001) direction, which is the energetically preferred direction without substrate influence. For higher temperatures the substrate-induced $(10\bar{1}1)$ orientation dominates.

Perpendicular to the $(10\bar{1}1)$ growth direction, Y$[11\bar{2}0]$ is parallel to Nb[010]. Comparing with the sapphire substrate orientation we find that the equivalent [001] direction of the fourfold Nb(100) plane is never chosen as the preferred orientation. We propose that the symmetry is destroyed by the steps which result from the Nb tilt.

4.2. Conclusions

Comparing AFM and x-ray studies we come to several conclusions.

(i) The surface roughness determined by AFM is comparable to the Y layer roughness measured by x-ray diffraction. This confirms that the facets develop in the Y layer, not in the flat buffer layer or in the cap layer.
(ii) The correlated diffuse intensity corresponds to a distance d which is comparable to the width of the facets $B = 280 \pm 110$ nm deduced from AFM line scans.
(iii) The correlated diffuse intensity is related to the facet structure, but only the width of the facet seems to be correlated while the diffuse scattering perpendicular to the facets shows no correlation. This can be explained by the different length of the facets which is not determined by special low-index crystal planes, while the width depends on the geometric form of the facets and can only vary with their height.

5. Discussion and growth model

Our experiments concerning the structure of Y$(10\bar{1}1)$/Nb(100) confirm the close relationship of this growth direction to Y$(10\bar{1}2)$/Nb(211):

(1) Both growth directions are slightly tilted with respect to the Nb lattice planes with the tilt direction perpendicular to Y$(11\bar{2}0)$.
(2) The facets found on both surfaces grow with increasing growth temperature while layer thickness and deposition rate remain constant.
(3) In both cases one of the facet surfaces originates from the tilted lattice plane.

In contrast to the predicted tilt angle of 1.197° for Y$(10\bar{1}1)$, we measured a surprisingly large angle of $\sim 2°$ (see figure 9). Nevertheless, applying the geometrical model has some justification. According to the model, the optimal dislocation net on Nb(211) is much narrower than on Nb(100), where we expect an average distance of 40 $a_{\mathrm{Nb}} \approx 130$ Å separating two dislocations compared to 28 Å on Nb(211). Consequently, unperturbed growth can only take place if the Nb sample possesses an ideal surface on the scale of the assumed dislocation net. In the case of Y on Nb(211) this condition is easily fulfilled because of the relatively short dislocation distance and the small substrate misfit, while for Y on Nb(100) a long-range order of the Nb surface is necessary. Therefore the step structure of the surface can perturb the dislocation net severely. From the measured tilt angle we deduce $n = 20$–30 which corresponds to a dislocation distance of 66–100 Å. For monatomic steps on Nb(100) we calculate from the misfit a step width of about 50 Å, which is of the same order as the calculated dislocation net. This suggests that Y$(10\bar{1}1)$ cannot reach the ideal dislocation net expected by the model because the steps modify the local stress. Considering the misfit reduction induced by the tilted Y$(10\bar{1}1)$ surface, we expect that a tilt of $\approx 2°$ will diminish the misfit from $f = -1\%$

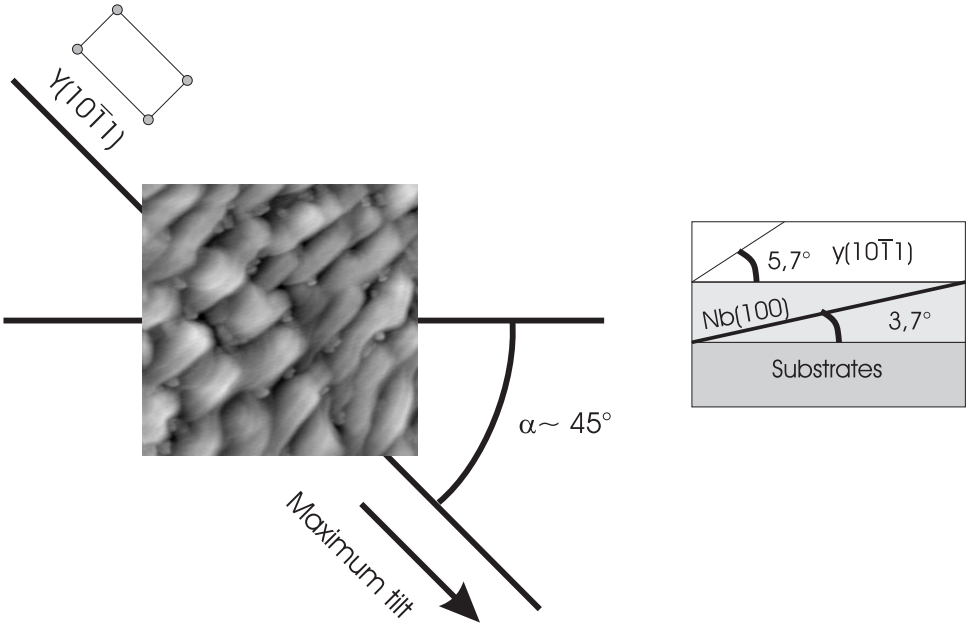

Figure 9. The relation of the maximum tilt direction of Y(10$\bar{1}$1) to the sample morphology. On the right-hand side a cross-section through the sample along the maximum tilt direction is presented.

to $f = -0.17\%$. This small residual value is possibly due to the perturbation by the steps. Furthermore, it is possible that the steps serve as pinning centres for the dislocations.

In this context an interesting situation arises: we can only explain the tilt by assuming dislocations which insert an element of the basal plane with the width $d_Y = (\sqrt{3}/2)a_Y$. For a number of hcp(10$\bar{1}$1) materials [11] the tilt angle can be calculated exactly with this model. We now discuss the different dislocation vectors in the basal plane [21]. The hcp Burgers vector $\boldsymbol{b}$ with the smallest dislocation energy points in the correct direction but then $b = (2/3)d = (\sqrt{2}/3)a_Y$ instead of $b = a_Y$ as assumed in the model. Assuming this dislocation type and using the geometrical model, we still cannot explain the tilt angle. The Burgers vector [10$\bar{1}$] with $b = a$ correctly explains the tilt angle but because $E \sim b^2$ this dislocation contains more energy. It will be interesting to determine by other methods whether this normally unfavourable dislocation takes place in thin films.

As shown by RHEED measurements, not only Y(10$\bar{1}$2) [3] but also Y(10$\bar{1}$1) develops a faceted surface during growth. Facets can be induced by stress [16, 17] or energy reduction of the relaxed crystal [16, 18, 19]. According to the geometrical model, in the ideal case the stress of the Y film is totally relieved by the tilt at the Y/Nb interface. Therefore the driving force for faceting must be energy reduction of a relaxed crystal. The energy of a real crystal surface consists of three contributions: (1) surface tension; (2) edge energy where two surfaces come together; and (3) the energy of points where three or more surfaces meet. A vicinal surface as produced by the tilt is energetically unfavourable because of the high step density. Consequently the steps bunch together forming large facets with fewer edges.

From the step bunching mechanism one would expect the Y(0001) plane to be a facet surface as well. In reality, for Y(10$\bar{1}$1) the (10$\bar{1}$3) lattice plane is found to be a facet surface. We explain this by the large angle of 42.2° between (10$\bar{1}$2) and (0001) while (10$\bar{1}$2) and (10$\bar{1}$3) are separated by only 6.7°.

The temperature dependence of the facets nicely corresponds to a Monte Carlo simulation performed by Vlachos *et al* [18]. Based on first- and second-nearest-neighbour interactions, this simulation models faceting of a simple cubic lattice depending on time, temperature and growth rate. Assuming constant growth rate and deposition time, the facet size grows with increasing temperature up to a critical thickness when thermal roughening commences. The experimental conditions that we used are clearly far away from the roughness transition temperature because the roughness increases while the facet structure is maintained. The simulation also shows the nearly periodic facet structure as experimentally observed.

Acknowledgments

This work was supported by the Deutsche Forschungsgemeinschaft, SFB 166, and by the Ministerium für Wissenschaft und Forschung des Landes Nordrhein–Westfalen, which is gratefully acknowledged. Furthermore, we thank K A Ritley for fruitful discussions.

References

[1] Kwo J, Hong M and Nakahara S 1986 *Appl. Phys. Lett.* **49** 319
[2] Huang J C A, Du R R and Flynn C P 1991 *Phys. Rev. Lett.* **66** 341
[3] Du R 1990 *Thesis* University of Illinois at Urbana-Champaign
[4] Bauer E and van der Merwe J H 1986 *Phys. Rev.* B **33** 3657
[5] *Handbook on the Physics and Chemistry of Rare Earths* 1978 ed K A Gschneidner Jr and L Eyring, vol 1 (Amsterdam: North-Holland)
[6] Majkrzak C F, Kwo J, Hong M, Gibbs D, Chien C L and Bohr J 1991 *Adv. Phys.* **40** 99
[7] Theis-Bröhl K, Ritley K A, Flynn C P, Van Nostrand J E, Cahill D G, Hamacher K, Kaiser H and Rhyne J J 1997 *J. Magn. Magn. Mater.* **166** 27
[8] Huiberts J N, Griessen R, Rector J H, Wijngarten R J, Dekker J P, de Groot D G and Koeman N J 1996 *Nature* **380** 231
[9] Huiberts J N *et al* 1996 *J. Alloys Compounds* **239** 158
[10] Remhof A, Song G, Theis-Bröhl K and Zabel H 1997 *Phys. Rev.* B **56** 2897
[11] Du R and Flynn C P 1990 *J. Phys.: Condens. Matter* **2** 1335
[12] Weschke E, Schüßler-Langheine C, Meier R, Kaindl K, Sutter C, Abernathy D and Grübel G 1997 *Phys. Rev. Lett.* **79** 3954
[13] Herman M A and Sitter H 1989 *Molecular Beam Epitaxy, Fundamentals and Current Status* 2nd edn (Berlin: Springer)
[14] Flynn C P 1988 *J. Phys. F: Met. Phys.* **18** L195
[15] Schmitte T 1997 *Diplomarbeit* Ruhr-Universität Bochum
[16] Liu F and Metiu H 1993 *Phys. Rev.* B **48** 5808
[17] Jesson D E, Chen K M and Pennycook S J 1996 *MRS Bull.* **21**
[18] Vlachos D G, Schmidt L D and Aris R 1992 *Phys. Rev.* B **47** 4896
[19] Desjonquères M C and Spanjaard D 1998 *Concepts in Surface Physics* 2nd edn (Berlin: Springer)
[20] Parratt L G 1954 *Phys. Rev.* **95** 359
[21] Bohm J 1995 *Realstruktur von Kristallen* 1st edn (Stuttgart: Schweizerbart)